# The BADC and BCCP subunits of chloroplast acetyl-CoA carboxylase sense the pH changes of the light–dark cycle

Yajin Ye<sup>1,2</sup>, Yan G. Fulcher<sup>1</sup>, David J. Sliman<sup>4</sup>, Mizani T. Day<sup>1,2</sup>, Mark J. Schroeder<sup>1,2</sup>, Rama K. Koppisetti<sup>1</sup>, Philip D. Bates<sup>4</sup>, Jay J. Thelen<sup>1,2</sup>, Steven R. Van Doren<sup>1,3\*</sup>

From the <sup>1</sup> Department of Biochemistry, 117 Schweitzer Hall, <sup>2</sup> Christopher S. Bond Life Sciences Center, 1201 Rollins Ave., <sup>3</sup> MU Institute for Data Science and Informatics, 241 Engineering Building West, University of Missouri, Columbia, MO 65211, and <sup>4</sup>Institute of Biological Chemistry, Washington State University, Pullman, WA 99164

Running title: pH sensing small subunits of plastid ACCase

\* address correspondence to Steven R. Van Doren, Dept. of Biochemistry, 117 Schweitzer Hall, University of Missouri, Columbia, MO 65211; <a href="mailto:vandorens@missouri.edu">vandorens@missouri.edu</a>

**Keywords**: biophysics, fatty acid biosynthesis, pH regulation, protein-protein interaction, lipid synthesis, nuclear magnetic resonance (NMR), thermodynamics, plant biochemistry, Arabidopsis, intrinsic disorder

#### **ABSTRACT**

Acetyl-CoA carboxylase (ACCase) catalyzes the first committed step in de novo synthesis of fatty acids. The multisubunit ACCase in the chloroplast is activated by a shift to pH 8 upon light adaptation and is inhibited by a shift to pH 7 upon dark adaptation. Here, titrations with the purified ACCase BADC and BCCP subunits from Arabidopsis indicated that they can competently and independently bind biotin carboxylase (BC), but differ in responses to pH changes representing those in the plastid stroma during light or dark conditions. At pH 7 in phosphate buffer, BADC1 and BADC2 gain an advantage over BCCP1 and BCCP2 in affinity for BC. At pH 8 in KCl solution, however, BCCP1 and BCCP2 had more than 10-fold higher affinity for BC than did BADC1. The pH-modulated shifts in BC preferences for BCCP and BADC partners suggest they contribute to light-dependent regulation of heteromeric ACCase. Using spectroscopy, we found evidence for increased intrinsic disorder of the BADC and BCCPs subunits at pH 7. We propose that this intrinsic disorder potentially promotes fast association with BC through a "flycasting mechanism." We hypothesize that the pH effects on the BADC and BCCP subunits attenuate ACCase activity by night and enhance it by day. Consistent with this

hypothesis, Arabidopsis *badc1 badc3* mutant lines grown in a light–dark cycle synthesized more fatty acids in their seeds. In summary, our findings provide evidence that the BADC and BCCP subunits function as pH sensors required for light-dependent switching of heteromeric ACCase activity.

In most plants (dicots and non-grass monocots), a multi-subunit, heteromeric carboxylase acetvl-CoA (hetACCase) resides in plastids to generate the malonyl-CoA required for *de novo* fatty acid synthesis (1, 2)(Fig. 1A). This first committed step of fatty acid synthesis controls carbon flow into the pathway and is thus highly regulated (1, 2). Newly synthesized fatty acids (FAs) are processed into glycerolipids for plant cell membranes or storage triacylglycerols (oils) within the seed or mesocarp. The varied markets for vegetable oils, including cooking and dietary oils, biodiesel and chemical feedstocks, motivates ongoing interest in engineering of oilseeds (3, 4) and the regulatory properties of hetACCase (5–7).

Formation of malonyl Co-A by ACCase was reported to be the only light-regulated step for *de novo* FA synthesis in plants (8). The activity of hetACCase in chloroplasts is increased in the light by the conditions created by the photosynthetic light

reactions, namely high ATP levels, a shift to pH to 8 in the stroma, and a pool of reduced thioredoxin that enhances hetACCase by reducing disulfide bonds within carboxyltransferase (CT) subunits (9-12). The first half-reaction of hetACCase is catalyzed by the biotin carboxylase (BC) subcomplex which uses bicarbonate and ATP to carboxylate the biotin cofactor of a biotin carboxyl carrier protein (BCCP; see 13-15). Fig. 1A)(2, 5. carboxyltransferase subcomplex of α-CT and β-CT subunits catalyzes the second halfreaction that transfers the carboxyl group from biotin to acetyl-CoA to form malonyl-CoA (2, 5, 13-15). The structural bases of the functions of the BC, BCCP, and CT subunits were reviewed (15). An oligomeric complex of the folded region of BCCP and BC subunits from the ACCase from E. coli was elucidated by crystallography (16). In plants, the malonyl-CoA pool in the plastid for de novo FA synthesis is distinct from the cytosolic malonyl-CoA pool used for FA elongation, which is generated by a separate homomeric ACCase (2).

BCCP-like biotin attachment domain-containing protein (At1g52670) was first described in 2009 (17) and subsequently named biotin attachment domain-containing 2 (BADC2) (6). The BADC1 and BADC3 members of this gene family were identified and were demonstrated to associate with the subcomplex containing BCCP1, BCCP2, and BC subunits of Arabidopsis (6). The mature BADC subunits at 22 to 24 kDa in mass (6) are slightly larger than the BCCP subunits of 18 to 21 kDa, and less than half the mass of the BC and CT subunits (Table S1). Although BADC subunits retain the sequence similarity of the biotin/lipoyl attachment domain, BADC1, BADC2, and BADC3 specifically lack the canonical four amino acid sequence motif for biotinvlation in BCCPs, and were experimentally shown to lack a covalently-bound biotin prosthetic group (6). Addition of excess BADC1, BADC2, or BADC3 to extracts from developing Arabidopsis siliques inhibited

hetACCase activity by about 37%, 33%, and 24%, respectively (6). Addition of BADC1 to leaf extracts inhibited ACCase activity up to ~27% in a concentration-dependent fashion (6). BADC subunits' lack of biotinylation and partial inhibition of hetACCase supports the hypothesis that BADC subunits inhibit by competing with BCCP subunits for access to BC (6). Partial RNAi silencing of BADC1 in Arabidopsis seeds increased seed oil content (6). Comparison of T-DNA knockout badc1 badc3 Arabidopsis with wild type found ACCase activity to be higher and seeds to contain 33% more triacylglycerols (TAGs) in badc1 badc3 lines (7). This suggests that relief of inhibition by BADC1 and BADC3 results in higher hetACCase activity and carbon flux through de novo FA synthesis (7). Potential mechanisms for BADC competition with BCCP subunits remain unclear. Results in Arabidopsis suggest that BCCP and BADC are capable of binding to BC somewhat independently (6, 7). However, this has yet to be demonstrated in quantitative fashion.

More roles for the BADC subunits in Arabidopsis have emerged recently. An important but unidentified role in seed development is indicated by the inability to obtain badc2 badc3 mutant seeds, as well as by the smaller seeds, roots, and rosettes of badc1 badc2 mutants (7, 18). The BADC1 and BADC3 subunits were implicated in long-term response to over-supply of FAs by feedback inhibition (7). When Arabidopsis BC was co-expressed in E. coli with Arabidopsis BCCP1 or BCCP2, a high level of co-expression also with a BADC subunit boosted BCCP recruitment of BC by more than 10-fold to nearly stoichiometric ratios in each of the BCCP-BADC-BC subcomplexes (18). The in vitro catalytic efficiencies and maximum catalytic velocities of the BCCP-BADC-BC subcomplexes reconstituted in E. coli were similarly elevated over those of their BCCP-BC counterparts, with BADC2 BADC3 and providing the biggest enhancement (18).

Assembly and stoichiometry macromolecular assemblies such as hetACCase is complex and often difficult to ascertain, given the need for absolute quantitation in vivo. The mass spectrometry approach known as Absolute QUAntitation of Multiplexed Reaction Monitoring (AQUA-MRM) provided the molar protein quantities of hetACCase subunits in Arabidopsis siliques when the seeds are actively filling with oil. The molar quantities of the subunits rank in the order  $\beta$ -CT > BC > BADC1 > BADC3 ≈ BCCP1 > α-CT ≈ BCCP2 > BADC2 (19). During oilseed development, BADC1 and BCCP1 being the most highly expressed of the non-biotinylated and biotinylated smaller subunits, respectively, merits study of their behaviors.

Illumination and the photosynthetic light reactions pump protons out of the chloroplast stroma, raising its pH from 7 to 8 (20). We focus herein on investigation of the hypothesis that the light-dependent swings in pH of the plastid stroma might regulate association of BCCP and BADC subunits with the biotin carboxylase subunit, which alters subcomplexes forms and the catalyzing carboxylation of biotinylated BCCP1 or BCCP2. We considered the possibility that the physiological pH range affects the BCCP and BADC subunits in terms of (i) their affinities for BC and (ii) their structural scaffolds in solution. The BADC and BCCP subunits associate with BC directly and independently with  $K_D < 10 \mu M$ under all solution conditions evaluated. The affinities are greater at pH 7 than at pH 8. The intrinsic disorder detected by NMR in pH titrations of BCCP1, BCCP2, and BADC1 is also increased at pH 7. At pH 7, enhanced BADC occupation of BC predicts that biotin carboxylation should be slower at pH 7. At pH 8, enhanced BCCP subunit occupation of BC predicts enhanced biotin-mediated transfer of carboxyl groups between the active sites of BC and CT subunits. Thus, the BCCP and BADC subunits sense pH and respond in a differential manner that may help (i) inhibit the biotin carboxylase halfreaction in the neutral pH of dark and low light conditions and (ii) accelerate biotin carboxylation in the pH 8 of light adaptation, and thereby enhance the light-dependent regulation of hetACCase in plastids. Consistent with these predictions and with the abundance of the BADC1 and BADC3 subunits, the seeds produced by Arabidopsis badc1 badc3 lines accumulate more total lipid when the lines are grown with a daily light/dark cycle.

#### Results

# Predictions of folded and disordered regions of plastid BCCP and BADC subunits

The approximately 90 residues at the C-terminal end of the BCCP1, BCCP2, BADC1, BADC2, and BADC3 sequences from A. thaliana exhibit homology to structures in the Protein Data Bank. Homology models, using crystallographic coordinates of BCCP from E. coli, contain two anti-parallel B-sheets in each of these subunits of acetyl-CoA carboxylase (Fig. 1B,C). Homology models of this region from each BADC subunit comprise eight βstrands, BCCP2 seven strands, and BCCP1 six strands plus a potential but ambiguous seventh strand at its C-terminus. At the Nterminal end of this region, the BADC subunits add a  $\beta$ -strand to one  $\beta$ -sheet (Fig. S1 and purple in Fig. 1C) while the corresponding segment of the BCCP1 and BCCP2 models is similar but diverges (Fig. S2B). The exposed "thumb" loop is much longer and enriched in basic residues in the models of the BADC subunits (Fig. 1C, S2B). The lysine in the  $\beta$ -hairpin loop that becomes biotinylated in BCCP subunits is replaced by glycine in the BADC subunits. Apart from localized differences at the termini and thumb, the backbone coordinates of the homology models are highly similar (Fig. S2).

Due to the small size of the folded regions, we examined the sequences of the mature BCCP1, BCCP2, BADC1, BADC2, and BADC3 subunits from *A. thaliana* for

disorder. The unusual structural, sequence. and functional properties of intrinsic disorder were reviewed (21). Intrinsically disordered regions (IDRs) exhibit elevated mean charge, low mean hydrophobicity, depletion of bulky hydrophobic side chains, and enrichment in disorder-promoting Pro, Glu, Ser, Lys, and Gln residues (21-23). The content of these five disorder-promoting residues ranges from 38% in BADC2 to 45% in BCCP1. We applied the CASP9-winning MetaDisorderMD2 approach that integrates multiple predictions of disorder (24, 25). These predictions suggest that a large IDR lies in the middle of each sequence. preceding the structured domain (Fig. 1D-H). The predictions also feature an N-terminal IDR followed by an ordered region of 20 to 30 residues. The "thumb" region of BADC1 is predicted to be an IDR (Fig. 1D-H). MetaDisorderMD2 suggests disorder for 59% of the residues of BCCP1, 56% of BCCP2, 62% of BADC1, 55% of BADC2, and 51% of BADC3. The BCCP subunits average a proline content of 14% while the BADC subunits average 7% proline. The proline residues, which promote extended structure, are concentrated in the large central IDR predicted, as well as in the thumb (Fig. S1). Glu and Asp residues comprise 11 to 12% of the amino acids of the BCCP and BADC subunits. The enrichment in negative charge provides electrostatic repulsion opposed to hydrophobic collapse (21).

### Affinities for BC respond to pH and ions

The question of the pH dependence of the BADC and BCCP subunits' affinities for the BC subunit arose from the pH-dependence of ACCase activity (10, 12) and from the sensitivity of the folds of BCCP1, BCCP2, and BADC1 to pH (see below). We monitored titrations of BC with BCCP1, BCCP2, BADC1, BADC2, or BADC3 by microscale thermophoresis (MST), which is sensitive to binding interactions. MST senses molecular interactions via the accompanying changes to molecular size,

charge, and hydration shell that respond to a temperature jump from an infrared laser pulse (26, 27). The changes in thermal molecular movement are detected by fluorescence, which is sensitive to modest amounts of the binding partners. We compared pH conditions representative of daylight (pH 8) and dark (pH 7). Good's buffers have been popular for assays of hetACCase activity (6, 18). However, the 1.2 to 2 mM phosphate (Pi) present in the stroma of chloroplasts fully active in photophosphorylation (28) suggests the relevance of phosphate-containing buffers. Hence, we also conducted titrations in PBS containing NaCl, or PBK containing KCl. [K<sup>+</sup>] in chloroplasts was reported to range from 40 mM in pea to 160 to 200 mM in spinach and sugarbeet, chloroplasts and [Na+] to range from 40 to 70 mM in pea, spinach and sugarbeet chloroplasts (29). Potassium ions are required for a high rate of photosynthesis (30). Titrations detected by MST suggest that the affinities for BC strongly depend on the ionic milieu (Fig. 2). Comparisons of the Gibbs free energies of association with BC clarify the effects of pH and choice of buffer (Fig. 3).

The drop in pH from 8 to 7 significantly increased BC affinities for each of the small sibling subunits in NaClcontaining solutions of PBS (rightward shifts in Fig. 3A). The BCCP subunits increased in affinity for BC by about 1 kcal/mol due to this change (Fig. 3B). BC affinity for BADC1, BADC2, and BADC3 increased at pH 7 by 2.1, 0.8, and 1.5 kcal/mol, respectively. Consequently, at pH 7 in NaCl and phosphate, BC affinity for BADC1 and BADC3 exceeded that in KCI and HEPES by 1.4 and 0.9 kcal/mol, respectively (Fig. 3A,C). BADC1 and BC reached a  $K_D$  of 54 nM at pH 7 in PBS (Table 1, Fig. 2C). These results can be regarded as enhancement of BADC1 and BADC3 affinity for BC at pH 7 by PBS (Fig. 3A,C). This behavior suggests that the combination of 40 to 70 mM Na<sup>+</sup> and 1 to 2 mM phosphate in the plastid (28, 29) with the pH 7 of dark conditions could enhance

occupation of BC by abundant BADC1. The likelihood of more occupation of BC by BADC1 at pH 7 could increase inhibition of hetACCase, because BADC1 lacks a biotin group needed for the biotin carboxylase half-reaction.

In KCI solution buffered by HEPES, BCCP1 affinity for BC exceeded that in PBS by 1.2 kcal/mol at pH 7 and by 2.2 kcal/mol at pH 8 (Fig. 3A,C). BCCP2 mimicked this at a smaller level. In HEPES-KCI, BCCP2 affinity for BC exceeded that in PBS by 0.7 kcal/mol at pH 7 and by 1.5 kcal/mol at pH 8 (Fig. 3A,C). In HEPES-KCI, the gain in affinity for BC with a drop in pH from 8 to 7 was limited to 1.2, 0.6, and 0.3 kcal/mol for BADC1, BADC2, and BADC3, respectively, and to 0.0 and 0.3 kcal/mol for BCCP1 and BCCP2 (Fig. 3B). In HEPES-KCI BCCP1 attained a  $K_D$  of about 45 nM for BC at either pH 7 or 8 (Table 1, Fig. 2A). KCl appeared to enhance the affinity of BCCP1 and BCCP2 for BC, relative to NaCl (Fig. 3A). In contrast, KCI seemed to detract from BADC1 affinity for BC and to do likewise at pH 7 to BADC3 (Fig. 3A).

Consequently, it appears as if Na<sup>+</sup> ions in the buffer tended to enhance BC affinities for the BADC subunits relative to BCCP1, whereas K<sup>+</sup> ions usually appeared to detract from the BC affinities of the BADC subunits relative to BCCP1 (Fig. 3D). This suggests that K<sup>+</sup> ions confer a preference of BC binding of BCCPs over BADC1 in the pH 8 of daylight conditions when hetACCase, FA synthesis, and photosynthesis are active.

Phosphate buffer at pH 8, compared to HEPES, detracted from BC affinity for BCCP1 by 1.6 kcal/mol and for BCCP2 and BADC1 by 0.4 kcal/mol (purple circles in Fig. 3C). In contrast, phosphate at pH 8 boosted BC affinity for BADC3 by 1.0 kcal/mol (Fig. 3C). This resulted in equivalent BC affinities for BCCP1, BADC1, and BADC3 at pH 8 in PBS (Table 1, Fig. 3A,D). The combination of KCl, phosphate, and pH 8 was equalizing to the BC affinities of BCCP1, BCCP2, BADC2, and BADC3, but diminished that of

BADC1 (Fig. 3D). At both pH 7 and 8, phosphate established more parity (compared to HEPES) among the BC affinities for BCCP and BADC subunits (triangles in Fig. 3D). The exceptions to the phosphate-promoted convergence in affinity for BC have potential to regulate hetACCase activity, i.e., Na<sup>+</sup> enhancements of the BC affinities of BADC1 and BADC2 at pH 7 and K<sup>+</sup>-diminished BC affinity for BADC1 at pH 8 (Fig. 3C).

## Evidence of partial unfolding at neutral pH and lower

The backbone amide region of NMR spectra is excellent for assessing the structural integrity and unfolding of proteins prepared with <sup>15</sup>N labeling of the peptide bonds (31, 32). NMR spectra of the BCCP and **BADC** subunits examined surprisingly sensitive to pH changes across the neutral range (Fig. 4) and suggest the extent of unfolding as pH drops. The spectra of the BCCP1, BCCP2, and BADC1 subunits in the range of pH 7.5 to 8 show the broad spread of backbone amide peaks expected of a folded domain (Fig. 4A,E,I, measured in PBS). In Fig. 4, most of the blue-colored peaks represent amide groups in folded parts of the proteins, whereas most of the red-colored peaks represent unfolded regions. The unfolded character associated with the red peaks is suggested by their position in random coil regions of the spectrum (31, 32), their sharp line widths. and growth with acidification of the samples. In contrast, the blue colored peaks in Fig. 4 probably include 65 or more residues predicted to adopt the β-sheet-containing fold in the C-terminal portions of the sequences. The random coil peaks of solvent-exposed sequences may, however, be broadened away by chemical exchange with the solvent water, and possibly by chemical exchange among conformers. Once the pH is titrated to the neutral range, additional amide NMR peaks at random coil chemical shifts appear (red contours in Fig. 4B,F,J), suggestive of partially unfolded forms present.

We sought to compare the pH dependence of partial and complete unfolding of BCCP1, BCCP2, and BADC1 quantitatively, based on the pH titrations monitored with NMR spectra. The size, extent, and unknown direction of the peak shifts upon acidification (Fig. 4) impede manual quantification. Fortunately, the pH dependencies of protein folding transitions have been derived reliably from NMR peak lists using the established chemometric strategy of principal component analysis (PCA) (33). Consequently, we used this mathematical approach to identify the pHdependent changes in folding from the NMR spectra of our pH titrations, using PCAbased software called TREND NMR (34, 35). We bypassed the peak picking step and applied the PCA directly to the series of NMR spectra, encouraged by the success of this direct approach in capturing ligand binding transitions (34, 36-39). This semi-automatic strategy simplified the complex NMR spectral changes to suggest the underlying pH-dependent unfolding transitions of BCCP1, BCCP2, and BADC1. The pHunfolding dependent transitions suggested by the two biggest principal components (PCs) of change among the spectra (35, 36). One transition suffices to fit PC1 derived from each titration, whereas two pH-dependent unfolding transitions are required to fit PC2 from each of the titrations. The midpoint of the higher conformational transition of BCCP1 is near pH 6.8 in PC1 and pH 7.45 in PC2 (Fig. 5A); this describes the appearance of peaks at random coil chemical shifts in the near-neutral pH range. The midpoint of the appearance of amide NMR peaks of BCCP2 at random coil positions is pH 5.0 in both PC1 and PC2 (Fig. 5B). This indicates that BCCP2 withstood mild acidification more robustly than did the more labile BCCP1. In the case of BADC1, the higher pH transition is resolved in PC2 with apparent midpoint of pH 5.2 (Fig. 5C). The fit to PC1 of the BADC1 titration also improved by including the pH 5.2 transition (as 17% of the change). The fitted pH titrations suggest the midpoint of partial

unfolding of BCCP1 may be as much as 1.8 pH units higher than in BCCP2 or BADC1. However, some partial unfolding of BCCP2 and BADC1 is also present near pH 6.8 (Fig. 4F,J). The partial unfolding transitions suggest BCCP1 to be the most susceptible to the pH 7 of dark-adapted chloroplast stroma. The relative structural integrity might account for the advantage of BADC1 over BCCP1 in affinity for BC at pH 7 in PBS (Figs. 2, 3C).

In order to compare the pH titrations quantitatively, we continued the titrations into the acid range. BCCP1 appeared to be fully unfolded below pH 5.3 (Fig. 4D), BCCP2 by pH 2.6, and BADC1 by pH 2.6. The midpoint fitted to the lower pH-dependent transition captured by PC2 corresponds to the disappearance of the amide NMR peaks of folded protein, i.e., apparent unfolding. The midpoint of pH 5.5 for the unfolding of BCCP1 is higher than the midpoints of unfolding of BCCP2 at pH 3.8 and BADC1 at pH 3.9 (Fig. 5). Thus, the fitting of the NMR spectral changes suggests BCCP1 to be the most vulnerable to both unfolding and partial unfolding by decreasing pH.

# Increased seed oil in badc1/3 mutant line grown with light-dark cycle

biophysical results The above suggest the hypothesis of BADC subunits dominating complexes with BC and inhibiting hetACCase activity under conditions of neutral pH expected in the plastid stroma in conditions of dark and low light. The comparatively high abundance of BADC1 and BADC3 (19) (Table S1) and recent results on the enhanced seed oil content of badc1 badc3 lines (7, 18), suggested that these two subunits may act importantly in inhibition of hetACCase during night and possibly light-dark transitions, i.e. at dawn and dusk. Therefore, we tested these hypotheses together by comparing Arabidopsis seed oil accumulation in wildtype, badc1 badc2, and badc1 badc3 double mutants grown under a light-dark cycle or under 24 hr of constant light (Fig. 6). In

general, plants grown at 24 hr light had higher seed weight and lipid content as compared to those grown with a 16/8 hr lightdark cycle, consistent with previous comparisons of seed lipid content from plants grown under constant light versus cycling between day and night conditions (40). When grown under a light-dark cycle, the badc1 badc3 mutant had a higher seed weight, FA content per seed, and FA content as a percentage of seed weight as compared to wild-type (Fig. 6A-C). However, there was no significant difference in seed weight or seed FA accumulation when the same lines were grown under constant light (Fig. 6D-H). This result suggests that the enhancement of seed FA biosynthesis in the badc1 badc3 double mutant is related to cycles of light and dark, which also produce cycles in plastid pH from 8 to 7.

#### **Discussion**

### Light-induced changes in pH and activity

The environment of the heteromeric ACCase in the chloroplast stroma is a scene of remarkable light-induced change, in which photosynthetic electron transport drives the pumping of protons to the thylakoid lumen to build the proton motive force (41) and the reduce NADP+ to NADPH for CO2 fixation (42). Illumination also increases stromal [Mg<sup>2+</sup>] to levels that increase hetACCase activity (10, 43). Thus, the heteromeric ACCase becomes more active when reduced carbon, Mg·ATP, and mildly alkaline pH stimulate de novo synthesis of FAs (10-12). We propose herein that the BADC and BCCP subunits act as pH sensors. Light increased FA synthesis over dark around three-fold in the absence of DTT (10). pH 8 increased malonyl-CoA formation over pH 7 around 10-fold with DTT (12). BADC1 can gain a six-fold advantage over BCCP1 in affinity for BC at pH 7 in PBS, which supplements its concentration advantage in plastids (Table 1 and S1, Fig. 7A). At pH 8 in KCI, BCCP1 and BCCP2 gain 13- to 100-fold and 18-fold, respectively, more affinity for BC than BADC1 (Table 1, Fig. S3).

Consequently, pH influences on affinities for BC could be important in pH regulation of hetACCase activity. The additional responsiveness of the activity to DTT and [Mg·ATP] that increased are photosynthetic light reactions need to be borne in mind (12, 18). Thus, the components of the BC sub-complex of ACCase can be hypothesized to sense the. conditions of active photosynthesis. Moreover, the appearance of BADC subunits evolution coincides with during emergence of several of the photosynthetic eukaryotes, namely the green algae with BADC3 and a red alga with BADC1 (6). Perhaps the evolution of BADC subunits enhanced the ability of the BC subcomplex to sense photosynthetic activity and to tune hetACCase activity in response.

With multiple BADC and BCCP subunits controlling activity of the biotin carboxylase half-reaction of the chloroplast ACCase (5-7, 18), we considered the responses of these subunits to the change in pH representing that of day-night cycles. Notable experimental observations herein include the following: (i) The BCCP and BADC subunits each bound directly and independently to BC in vitro with < 10  $\mu$ M  $K_D$ under all solution conditions evaluated. (ii) Neutral pH, especially in PBS, enhanced the affinities for BC (Fig. 3B). (iii) The affinity of BADC1 for BC increases the most as pH drops to 7 (Fig. 3A). (iv) BCCP1 and BCCP2 each gain at least an order of magnitude more affinity for BC than BADC1 at pH 8 in KCI (Table 1, Fig. S3), (v) More than half of each BCCP and BADC sequence from Arabidopsis appears likely to be disordered (Fig. 1). (vi) Dropping to neutral pH enhances the partial unfolding of the BCCP1, BCCP2, and BADC1 subunits that is predicted across more than half of each sequence (Fig. 1, 4, 5), BCCP1, BCCP2, and BADC1 show more NMR peaks at random coil chemical shifts near pH 7 (Fig. 4B,F,J). The very marginal stability of the folded domains and their sensitivity to solution conditions is consistent with the small folding core (Fig. 1).

### BADC1 should dominate and inhibit BC at neutral pH in low light conditions

Calculations using the  $K_D$  values and concentrations of the subunits present in plastids (Table 1, S1) predict that most of each BCCP or BADC subunit should be capable of binding BC (Fig. 7A). The ability of individual BCCP and BADC sibling subunits to bind the BC subunit in vitro with comparable affinities (Table 1, Fig. 3C) is noteworthy because in vivo concentrations of BC (83 fmol/µg protein) are lower than the collective abundance of BCCP and BADC subunits (121 fmol/µg protein; Table S1). This suggests the possibility of competition among sibling BCCP and BADC subunits to bind fewer BC subunits. The bacterial ACCase complexes may be regarded as models for the hetACCase from plants. A 1:1 ratio of BCCP to BC subunits was proposed the enzyme from Pseudomonas citronellolis (44), but a 2:1 ratio in the enzyme E. coli (45).However, from the crystallographic structure of the subcomplex from E. coli displays 4 BCCP subunits bound to 4 BC subunits, arranged as a dimer of dimers (16); see Fig. 7B. If a 1:1 ratio of BCCP to BC generalizes to hetACCase in plastids, the almost 50% excess of BCCP and BADC subunits over BC subunits in siliques from Arabidopsis (Table S1) suggests than not all BADC and BCCP can bind concurrently to the smaller pool of BC subunits. We discuss potential implications of pH sensing by these small sibling subunits upon affinities for BC.

Addition of exogenous BADC1 to excess attenuated hetACCase activity (6). Endogenous BADC1 already enjoys enough of a concentration advantage to dominate the binding of BC in PBS relative to its sibling subunits (Fig. 7A). This advantage is extended in two ways: First, the BADC subunits together enjoy an approximately 2.5-fold concentration advantage over the BCCP subunits in developing siliques (Table S1). Second, BADC1 exhibited a clear advantage in affinity for BC over the BCCP subunits at pH 7 in PBS (Fig. 3A,D)

Consequently, BADC subunits, led by BADC1 and lacking biotinylation, offer means of inhibiting hetACCase, especially during dark adaptation when the enzyme is less active.

BADC1 also underwent the biggest increases in affinity for BC as pH dropped from 8 to 7, which accompanies dark adaptation of plastids. The 35-fold increase in the BC affinity for BADC1 induced by the pH drop in PBS (Fig. 2C, 3A,B) corresponds to 2.1 kcal/mol (Fig. 3B). The results in phosphate-containing buffers seem more relevant than those in HEPES because the plastid stroma may contain up to 2 mM phosphate (28). BADC1 enjoys 1.1 and 1.3 kcal/mol advantages in affinity for BC over those of BCCP1 and BCCP2, respectively, at pH 7 in PBS (Table 1, Fig. 3A,C). Since BADC3 shares with the BCCPs similar protein expression levels in developing siliques and similar affinity for BC in PBS (Fig. 7A), BADC3 may also compete (or collaborate through heterodimerization (18)) with BCCP subunits in binding BC. This is corroborated by badc1 badc3 Arabiopsis strains grown with cycles of light and dark (Fig. 6A-C).

pH 8 detracted from BADC1 affinity for BC significantly, especially with KCI present (Fig. 2C, 3A-C). Consequently, at pH 8 in KCI, BADC1 is predicted to lose much of its physiological advantage in saturating BC (Fig. 7A). In HEPES-KCI, BCCP1 and BCCP2 held the advantage in BC affinity over BADC1 and BADC3, especially at pH 8 (Fig. 3A,C). [K+] being 160 to 200 mM in physiological plastids (29)suggests relevance for these observations. Consequently, in light-adapted plastids at pH 8 or higher, BCCP1 and BCCP2 should become more competitive with BADC1 in populating BC (Fig. 7). This should enhance ACCase activity while the proton pumping activity of the photosynthetic light reactions is active during daylight.

Switching of roles of BADC subunits?

Nearly normal to enhanced synthesis of FAs by badc1 badc2 and badc1 badc3 lines of Arabidopsis implies assembly of active BC subcomplexes despite a shortfall of BADC subunits (Fig. 6). This supports the view that BADC subunits, which lack biotin, may competitively inhibit biotin carboxvlase (5-7). However, reconstitution in E. coli of Arabidopsis BC and BCCP subunits together to a stoichiometric degree requires coexpression with a BADC subunit (18). Moreover, E. *coli-*expressed BC subcomplexes have substantially higher carboxvlase biotin activity reconstituted by co-expressing the BADC2 or BADC3 subunits (18). These observations suggest that BADC subunits recruited BCCP subunits to BC in E. coli. Can the contrasting evidences for competitive inhibition and activation of Arabidopsis hetACCase by BADC subunits both be accommodated?

The similarity of BC affinities for the BCCP and BADC subunits in phosphate buffer (Fig. 3D, Table 1) suggests that the siblings should bind BC concurrently. Since pH 8 weakens the BC affinity of all five siblings (Fig. 3A,C), the BCCP subunits, being less concentrated in plastids (19), might increase in association with BC at pH 8 if more abundant BADC subunits recruit them. The known heterodimerization of BCCP and BADC subunits (6, 18) makes joint recruitment to BC more plausible. Heterodimerization conceivably has another value in *E. coli*. The level of BCCP1 expression in E. coli tends to pass through an early peak 2 to 4 hours after induction. followed by a drop around 6 hours (Fig. S4). This suggests some degradation of BCCP1 in E. coli. Since the disordered N-terminus of BCCP1 interacts with a BADC subunit (18), it is possible that the heterodimerization may partially protect BCCP1 from proteolysis, and thereby ferry BCCP1 more successfully to its BC partner.

We lack evidence in plastids to evaluate BCCP-BADC heterodimers in physiological regulation of the activity of BC subcomplexes.\_Our simplified titrations *in* 

vitro again suggest that: (i) at pH 7 in phosphate buffer, the more abundant BADC1 could be dominant in association with BC in dark-adapted plastids and (ii) at pH 8 in KCl solution, BADC1 may lose its dominance in BC subcomplexes to BCCP1 and BCCP2 having one to two orders of magnitude more affinity for BC in light-adapted plastids (Table 1, Fig. 3, 7, S3).

### Functional advantages expected from the disorder of BCCP and BADC subunits

The intrinsic disorder of the BCCPs and BADCs and the higher affinities for BC at pH 7 should have biophysical implications. Intrinsic disorder is observed in multi-protein complexes and confers promiscuity to the protein-protein interactions of hub proteins Flexible peptides and intrinsically disordered proteins enjoy fast on-rates and off-rates in their associations with protein partners (46, 47). The speed of their association is attributable to fast zipping up due to the cooperative addition of many weak contacts at the interface (47, 48). The "fly-casting" model argues that intrinsic disorder increases the radius for capturing the partner with weak contacts to begin a molecular encounter complex (49, 50). The multiple weak protein-protein contacts typically combine with folded domains to accumulate affinity for protein partners (46). The IDRs of the BCCP and BADC subunits may also be hypothesized to confer affinities for other subunits of hetACCase. Consider the two biggest predicted IDRs in each BCCP and BADC, i.e., the central sequence of 50 and the N-terminus (Fig. 1). The Nterminal 70 residues of BCCP1 is required for its heterodimerization with BADC3 (18). A region of 48 residues from the disordered central IDR of BCCP1 appears to enhance association with BADC3, while the folded Cterminal region did not participate (18).

Potential protein binding regions residing in IDRs can be predicted using the ANCHOR method (51, 52). The ANCHOR method predicts that the principal IDR in BCCP1, BCCP2, and BADC1 may have two

regions for protein associations, but only one such site in the main IDR of BADC2 and BADC3 (Fig. 1, open circles). Additional partial unfolding apparent at near-neutral pH in the amide NMR spectra of Arabidopsis BCCP1, BCCP2, and BADC1 suggest that pH 7 possibly enhances their capture radii and exposure of protein binding regions beyond that at pH 8. This might increase the number of multivalent contacts possible with BC. Such enhancements might account for the higher affinities of the BCCP and BADC subunits for BC at pH 7 than at pH 8.

While NMR spectra reveal partial unfolding of the folded domain by neutral pH (Fig. 4), how much of the chains of BCCP and BADC subunits sense pH changes is less clear. The folded domains could sense the pH changes directly. In the homology models, basic and acidic side chains appear to be interspersed for favorable attractions. Partial protonation of these acidic side chains might decrease these stabilizing interactions. Yet the folded domains could also be influenced indirectly by the IDRs. The IDRs may sense pH changes because IDRs are highly charged and responsive to pH and counterions (21, 53). Since the anionic IDRs may be attracted to the basic thumb in each BADC subunit, there may be possibilities for IDRs to indirectly stabilize the folded domains in a pH-dependent fashion. The interaction of the N-terminal 71 residues of BCCP1 with BADC3 (18) might be compatible with the basic thumb of BADC3 attracting the net negative charge of this disordered part of BCCP1.

Under conditions of high activity at pH 8 in KCl, how can BC select the BCCP1 and BCCP2, needed for the activity, over BADC1 that is more abundant in plastids? At pH 8 in KCl, BC affinities for BCCP1 and BCCP2 were as little as 1.5 kcal/mol better than that of BADC1 (Table 1). Theory of promiscuous protein-protein associations pointed out that discrimination among alternative partners with small differences in affinity is maximized by modest affinities; the discrimination is maximal when  $K_D$  lies within

an order of magnitude of the concentrations of the partners (54). Fig. S3 suggests that this regime optimizes the BC preference for BCCP1 and BCCP2 over BADC1 or BADC3 at pH 8 in KCl, because the  $K_D$  values approach the physiological concentrations.

# Agreement of biophysical data with seed oil in badc1/3 lines grown in light-dark

The badc1 badc3 line grown in a day/night cycle had an ~18% increase in FAs per seed and an ~8% increase in seed weight producing an ~10% increase in seed lipid content by dry weight (Fig. 6). Previously, badc1 badc3 also grown under a day/night cycle was reported to have an ~9% increase in FAs per seed and an ~17% decrease in seed weight producing ~30% increase in seed lipid content by dry weight The reasons for the differential increase/decrease in seed weight are not clear but are likely due to other differences in growth conditions such as fertilizer, humidity, and especially light intensity of which is known to have a large effect on oilseed development (40). However, both studies indicate the badc1 badc3 mutant has a higher FA content when grown under a day / night cycle.

Comparison of affinities for BC suggests BADC subunits (Fig. 2, Table 1) should be more effective inhibitors at neutral pH conditions expected in chloroplasts in dark, dawn, and dusk conditions. High protein levels of BADC1 and BADC3 during seed development (19) draw attention to them. pH 8-enhanced competitiveness of BCCP1 and BCCP2 for BC (Fig. 3D, S3) may facilitate the higher catalytic turnover of carboxylated BCCP by BC during high activity at pH 8 of light adaptation. The increased seed oil content of badc1 badc3 mutant Arabidopsis grown with a light-dark cycle is in accord with these expectations. A low level of BADC2 protein expression relative to BADC3 (19)(Fig. 7A) could account for the lack of impact of the badc1 The inhibition of badc2 mutant line. hetACCase and FA synthesis by BADC1 and

BADC3 expected in the dark and low light of wild-type is relieved by the *badc1 badc3* double mutation (Fig. 6). BADC1 and BADC3 can be predicted to be less competitive with BCCP1 and BCCP2 during the pH 8 (Fig. S3) of constant illumination and continuing high activity of hetACCase. Consistent with this, the *badc1 badc3* double mutant had little impact on seed oil during growth under constant illumination (Fig. 6).

Conclusions -- The BADC and BCCP subunits of hetACCase appear to act as pH sensors. Amid the overall weaker affinities for BC at pH 8, BCCP1 and BCCP2 gained more than 10-fold advantages in affinity for BC over BADC1 (in KCl solutions). The pH 8 boost to BC preferences for BCCP1 and BCCP2 seems favorable for the activity of hetACCase in daylight. The decrease of pH from 8 to 7 increased the affinities of BADCs and BCCPs for the BC subunit of hetACCase, with BADC1 undergoing the greatest boost to affinity in PBS. The high physiological concentration and high BADC1 affinity for BC at pH 7 in PBS suggests BADC1 may be a principal inhibitor of biotin carboxylase activity in the dark. The intrinsic disorder of the BADC and BCCP subunits is likely to promote fast association with BC. If BADC subunits mediate inhibition by night and if BCCP subunits are enhanced in their with BC under interactions daylight conditions, that would implicate BADCs in light- and pH-dependent switching of hetACCase activity. Consistent with this switching hypothesis, the badc1 badc3 mutant line of Arabidopsis grown with a daily cycle of light and dark synthesizes more FAs in its seeds.

### **Experimental Procedures**

Disorder predictions. The mature sequences of the BCCP1, BCCP2, BADC1, BADC2, and BADC3 subunits of the het ACCase of *A. thaliana* were submitted to the GeneSilico server and its MetaDisorderMD2 algorithm for series of disorder calculations (25). MetaDisorderMD2 integrates predictions from 13 disorder predictors with

several structure-based predictions to enhance the sensitivity and specificity of the disorder prediction (25). The sequences of the subunits were also submitted to the IUPred2A server to obtain ANCHOR2 predictions of disordered binding regions for proteins (51, 52).

Sequence alignment and structural modeling. Multiple sequence alignment of the BADC and BCCP sequences from Arabidopsis was performed using Clustal Omega (55). The homology models were constructed with SWISS-MODEL (56, 57) at https://swissmodel.expasy.org/

Crystallographic coordinates of E. coli BCCP (PDB: 4HR7)(16) served as the template for building the homology models of BCCP1, BCCP2, BADC1, BADC2, and BADC3 from A. thaliana. Hypothetical BADC1 docking into tetrameric BC subcomplexes exploited structural alignment of its homology model with the BCCP coordinates in the crystal structure of the BC subcomplex from E. coli (16) using the align function in Pymol (58). The locations of the secondary structures predicted by the homology models were on the multiple rendered sequence alignment using the ESPript server (59).

Protein samples for MST. E. coli BL21 harboring pET28A expression vectors with inserts for the coding frames for Arabidopsis BC, BCCP1, BCCP2, BADC1, BADC2, or BADC3 were prepared previously (6). Each protein was expressed in Luria Broth containing either kanamvcin. Expression was induced with 100 µM IPTG when OD600 reached around 0.6. After a 6hour induction period, the cultures were pelleted and resuspended with 10 mL of lysis buffer (137 mM NaCl, 2.7 mM KCl, 10 mM Na<sub>2</sub>HPO<sub>4</sub> and 2 mM KH<sub>2</sub>PO<sub>4</sub>, pH 7.4, designated PBS). After cell disruption by French press and centrifugation to pellet the cell debris, the supernatant was incubated with 1 mL of nickel agarose resin (Gold Biotechnology, H-320). After 30-min. at 4 °C, the protein mixture was loaded onto a column of the nickel agarose and washed with 50 mL of wash buffer (20 mM imidazole

in Ivsis buffer, pH 7.4). After washing, the protein was eluted with 10 mL elution buffer (150 mM imidazole in lysis buffer, pH 7.4). The protein samples were purified to more than 90% purity and concentrated to around 500 µL with a Pierce concentrator PES with a 10,000 Dalton cutoff (ThermoFisher, 88527), according to the user manual. The buffers of the concentrated samples were changed by dialysis using dialysis vials (Sigma, PURN12030) overnight at 4 °C. After dialysis, the protein concentration was measured using the Bradford assay by reading A<sub>595</sub>. Bovine gamma globulin (ThermoFisher, 23212) was used to make a standard curve. The Bradford assay was calibrated against amino acid analysis quantified for 17 amino acids without Trp;

https://aescl.missouri.edu/MethRefs.html#aminoacids. The calibration used the theoretical molecular weight from the ExPASy server (60) using the mature sequences based on removal of the chloroplast transit sequence predicted using the ChloroP server (61).

Microscale thermophoresis (MST) was used to measure the affinity of the protein-protein interactions between BC and small subunits quantitatively. The His tag of 100 nM BC was fluorescently labeled using NanoTemper MO-L008 **RED-tris-NTA** according to the user manual., 10 µL of labeled BC protein was mixed with 10 µL of unlabeled small subunits (with serial dilutions in the same buffer). After at least 30 min., the samples were loaded into glass capillaries (NanoTemper, MO-K022). MST was carried out using 100 % LED power and high MST power with a NanoTemper monolith NT.115 instrument. The data were fitted and plotted using Origin 2019 or 2020 (OriginLab, Northampton, Massachusetts). The binding isotherms were fitted to a hyperbolic function of ligand concentration [L] with free parameters of dissociation constant ( $K_D$ ) and maximal binding  $B_{max}$  at saturation (62):

$$y = \frac{B_{max}[L]}{K_D + [L]} \qquad (1)$$

However, a few of the BADC1 binding isotherms were biphasic. The high affinity transition of interest was fitted better once a second term was added to accommodate the low affinity transition that did not saturate:

$$y = \frac{B_{max1}[L]}{K_{D1} + [L]} + \frac{B_{max2}[L]}{K_{D2} + [L]}$$
 (2)

The  $K_D$  values measured in phosphate were used to estimate the physiological fraction of BC bound,  $f_{bd}$ , by a single BCCP or BADC subunit, present at concentration  $L_t$ , using eq. 3:

$$f_{bd} = \frac{K_D + L_t + P_t + \sqrt{(K_D + L_t + P_t)^2 - 4P_tL_t}}{2P_t}$$

(3)

The total molar concentration of BC,  $P_t$ , was estimated as the 83 fmol/µg total protein measured in developing siliques (19), multiplied by the 400 mg of total protein/ml observed in plastids (63).  $L_t$  estimates of concentrations of the BCCP or BADC subunits in plastids were estimated similarly using the quantities in Table S1 scaled up by the 400 mg/ml protein present in plastids.

sample preparation. BADC1 coding frame was optimized for expression in E. coli using the IDT tool and subcloned into pET27B(+). 15N labeled Arabidopsis BCCP1, BCCP2 and BADC1 were prepared by culturing the E. coli BL21 with pET28a in PG minimal medium (64) prepared with 15N NH<sub>4</sub>Cl from (Cambridge Isotope Laboratories). The <sup>15</sup>N-labeled samples of Arabidopsis BCCP1, BCCP2, and BADC1 were prepared 150 to 180 µM in PBS buffer with composition listed above, but set to pH 8. The titration in Fig. 5A used 500 µM BCCP1, however.

pH titrations by NMR and their fitting. BEST-TROSY spectra (65) of the <sup>15</sup>N-labeled samples at 25 °C in 3 mm tubes (Norell) were collected using a Bruker Avance III 800 MHz NMR spectrometer. Starting with the samples near pH 8, small

aliquots of 0.1 N HCl or citric acid were added, pH read using a narrow glass electrode, and BEST-TROSY spectra collected with progressively lower pH as far as pH 2.6. Buffering of the pH in the acidic range was provided by the abundance of carboxylic acids in the protein chain, i.e. 24 in BCCP1, 20 in BCCP2, and 27 in BADC1. The NMR spectra were read and principal component analysis calculated TRENDNMR.exe, while the response v of each principal component (PC) was fitted to equation 4 or 5 using TRENDanalysis.exe (34, 35). Each fitted PC from the pH titrations was plotted in OriginLab 2019 or 2020. The pH transitions were fitted to equations similar to those reported (66, 67), featuring a midpoint  $(pK_{mid})$  in each pH transition captured by the PC from the titration. PC1 from each pH titration was monophasic and was fitted to a single term:

$$y = \frac{y_{max} - y_{min}}{1 + 10^{(pK_{mid} - pH)}}$$
 (4)

Fitting PC2 from the pH titrations required two terms opposite in sign (and  $y_{max1} \approx y_{max2}$ ):

$$y = y_{min} + \left[ \frac{y_{max1} - y_{min}}{1 + 10^{(pK_{mid1} - pH)}} \right] + \left[ \frac{y_{max2} - y_{min}}{1 + 10^{(pH - pK_{mid2})}} \right]$$
 (5)

Fits of PC2 from the titrations to eq. 5 optimized  $y_{min}$  to -0.47 for BCCP1 and BCCP2 and -0.52 for BADC1.

Light-dark cycle vs constant light grown seed oil measurements. Seeds were sterilized (with 70% ethanol for 5 min, 10% bleach with 0.1% SDS for 15 min, and washing 5 times with sterile water) and applied to germination plates (1x MS salts, 0.05% MES free acid, 1% sucrose, and 0.8% Agar, pH 5.7). The plates were incubated at 4°C for two days then placed under 24 hours of low light conditions of around 100 µmol photons m<sup>-2</sup> s<sup>-1</sup> light until all lines germinated and produced two true leaves (approximately 7-10 days). The seedlings were then transferred to soil and placed in either: (1) 16/8 hr light/dark cycle with 150-175 µmol photons m<sup>-2</sup> s<sup>-1</sup> light intensity at pot height measured across the

chamber: or (2) 24 hr constant light of 180-200 µmol photons m<sup>-2</sup> s<sup>-1</sup>. Both growth chambers used Full Spectrum Ceramic MH 315W bulbs and were set at a constant 23°C. All plants were watered as needed and fertilized twice a week with General Purpose mix NPK 20-10-20 (57.4 g/gal). For each light treatment, 18 individual plants of each plant line were grown together to provide seeds for analysis. Their locations were randomized across the growth chamber to minimize the effects of position within the chamber. Seed lipid content was determined by direct conversion to FA methyl esters (FAMEs) and quantification by gas chromatography with flame ionization detection based on ref (68). In brief, dry seeds were counted (n = 100) and weighed. FAMEs were produced in 1.5 ml 5% sulfuric acid in methanol at 85°C for 1.5 hr together with 50 µg 17:0 TAG in 0.2 ml toluene as an internal standard. FAMEs were extracted with 0.2 ml hexane and 1.5 ml 0.88% potassium chloride. The hexane phase was analyzed on an Agilent 7890B GC-FID with a DB-FATWAX UI column (30m, 0.25mm ID,  $df = 0.25 \mu m$ ) with He carrier gas at constant linear velocity 28.5cm/s, 100°C for 0 min, increased at 25°C/min to 200°C, then increased at 10°C/min to 240°C where held for 4.5 min. All calculations were done with Microsoft Excel, graphing and statistical analysis was done with GraphPad Prism version 8.3.

Data availability: All fitted and interpreted data are presented in the manuscript. The following data used for fitting are available upon request: (i) the MST titration data of Fig. 2 in text format and (ii) the raw and Fourier-transformed NMR spectra used in Fig. 4 and 5 in Bruker format. Send requests to: Steven Van Doren, email: <a href="mailto:vandorens@missouri.edu">vandorens@missouri.edu</a>, Biochemistry Dept., UMC, 117 Schweitzer Hall, Columbia, MO 65211 USA.

**Acknowledgments** -- We are grateful to T.P. Mawhinney for amino acid analysis and A. Bogner and A. Paz Herrera for exploratory protein preparations.

**Conflict of interest**: The authors declare that they have no conflicts of interest with the contents of this article.

#### Literature Cited

- 1. Ohlrogge, J. B., and Jaworski, J. G. (1997) REGULATION OF FATTY ACID SYNTHESIS. *Annu. Rev. Plant Physiol. Plant Mol. Biol.* **48**, 109–136
- 2. Sasaki, Y., and Nagano, Y. (2004) Plant Acetyl-CoA Carboxylase: Structure, Biosynthesis, Regulation, and Gene Manipulation for Plant Breeding. *Biosci. Biotechnol. Biochem.* **68**, 1175–1184
- 3. Thelen, J. J., and Ohlrogge, J. B. (2002) Metabolic Engineering of Fatty Acid Biosynthesis in Plants. *Metab. Eng.* **4**, 12–21
- 4. Cahoon, E. B., Shockey, J. M., Dietrich, C. R., Gidda, S. K., Mullen, R. T., and Dyer, J. M. (2007) Engineering oilseeds for sustainable production of industrial and nutritional feedstocks: solving bottlenecks in fatty acid flux. *Curr. Opin. Plant Biol.* **10**, 236–244
- 5. Salie, M. J., and Thelen, J. J. (2016) Regulation and structure of the heteromeric acetyl-CoA carboxylase. *Biochim. Biophys. Acta Mol. Cell Biol. Lipids.* **1861**, 1207–1213
- 6. Salie, M. J., Zhang, N., Lancikova, V., Xu, D., and Thelen, J. J. (2016) A Family of Negative Regulators Targets the Committed Step of de Novo Fatty Acid Biosynthesis. *Plant Cell.* **28**, 2312–2325
- 7. Keereetaweep, J., Liu, H., Zhai, Z., and Shanklin, J. (2018) Biotin Attachment Domain-Containing Proteins Irreversibly Inhibit Acetyl CoA Carboxylase. *Plant Physiol.* **177**, 208–215
- 8. Nakamura, Y., and Yamada, M. (1979) The light-dependent step of de novo synthesis of long chain fatty acids in spinach chloroplasts. *Plant Sci. Lett.* **14**, 291–295
- 9. Harwood, J. L. (1988) Fatty Acid Metabolism. *Annu. Rev. Plant Physiol. Plant Mol. Biol.* **39**, 101–138
- 10. Sauer, A., and Heise, K.-P. (1983) On the Light Dependence of Fatty Acid Synthesis in Spinach Chloroplasts. *Plant Physiol.* **73**, 11–15
- 11. Sauer, A., and Heise, K.-P. (1984) Regulation of Acetyl-Coenzyme A Carboxylase and Acetyl-Coenzyme A Synthetase in Spinach Chloroplasts. *Zeitschrift für Naturforsch. C.* **39**, 268–275
- 12. Sasaki, Y., Kozaki, A., and Hatano, M. (1997) Link between light and fatty acid synthesis: Thioredoxin-linked reductive activation of plastidic acetyl-CoA carboxylase. *Proc. Natl. Acad. Sci.* **94**, 11096–11101
- 13. Cronan Jr, J. E., and Waldrop, G. L. (2002) Multi-subunit acetyl-CoA carboxylases. *Prog. Lipid Res.* **41**, 407–435
- 14. Reverdatto, S., Beilinson, V., and Nielsen, N. C. (1999) A Multisubunit Acetyl Coenzyme A Carboxylase from Soybean. *Plant Physiol.* **119**, 961–978
- 15. Waldrop, G. L., Holden, H. M., and Maurice, M. St. (2012) The enzymes of biotin dependent CO2 metabolism: What structures reveal about their reaction mechanisms. *Protein Sci.* **21**, 1597–1619

- 16. Broussard, T. C., Kobe, M. J., Pakhomova, S., Neau, D. B., Price, A. E., Champion, T. S., and Waldrop, G. L. (2013) The three-dimensional structure of the biotin carboxylase-biotin carboxyl carrier protein complex of E. coli acetyl-CoA carboxylase. *Structure*. **21**, 650–657
- 17. Chen, M., Mooney, B. P., Hajduch, M., Joshi, T., Zhou, M., Xu, D., and Thelen, J. J. (2009) System Analysis of an Arabidopsis Mutant Altered in de Novo Fatty Acid Synthesis Reveals Diverse Changes in Seed Composition and Metabolism. *Plant Physiol.* **150**, 27–41
- 18. Shivaiah, K. K., Ding, G., Upton, B., and Nikolau, B. J. (2020) Non-Catalytic Subunits Facilitate Quaternary Organization of Plastidic Acetyl-CoA Carboxylase. *Plant Physiol.* **182**, 756–775
- 19. Wilson, R. S., and Thelen, J. J. (2018) In Vivo Quantitative Monitoring of Subunit Stoichiometry for Metabolic Complexes. *J. Proteome Res.* **17**, 1773–1783
- 20. Werdan, K., Heldt, H. W., and Milovancev, M. (1975) The role of pH in the regulation of carbon fixation in the chloroplast stroma. Studies on CO2 fixation in the light and dark. *Biochim. Biophys. Acta Bioenerg.* **396**, 276–292
- 21. Uversky, V. N., and Dunker, A. K. (2010) Understanding protein non-folding. *Biochim. Biophys. Acta Proteins Proteomics.* **1804**, 1231–1264
- 22. Uversky, V. N., Gillespie, J. R., and Fink, A. L. (2000) Why are "natively unfolded" proteins unstructured under physiologic conditions? *Proteins Struct. Funct. Bioinforma.* **41**, 415–427
- 23. Campen, A., Williams, R. M., Brown, C. J., Meng, J., and Dunker, V. N. U. and A. K. (2008) TOP-IDP-Scale: A New Amino Acid Scale Measuring Propensity for Intrinsic Disorder. *Protein Pept. Lett.* **15**, 956–963
- 24. Noivirt-Brik, O., Prilusky, J., and Sussman, J. L. (2009) Assessment of disorder predictions in CASP8. *Proteins*. 10.1002/prot.22586
- 25. Kozlowski, L. P., and Bujnicki, J. M. (2012) MetaDisorder: a meta-server for the prediction of intrinsic disorder in proteins. *BMC Bioinformatics*. **13**, 111
- 26. Jerabek-Willemsen, M., Wienken, C. J., Braun, D., Baaske, P., and Duhr, S. (2011) Molecular Interaction Studies Using Microscale Thermophoresis. *Assay Drug Dev. Technol.* **9**, 342–353
- 27. Seidel, S. A. I., Dijkman, P. M., Lea, W. A., den Bogaart], G. [van, Jerabek-Willemsen, M., Lazic, A., Joseph, J. S., Srinivasan, P., Baaske, P., Simeonov, A., Katritch, I., Melo, F. A., Ladbury, J. E., Schreiber, G., Watts, A., Braun, D., and Duhr, S. (2013) Microscale thermophoresis quantifies biomolecular interactions under previously challenging conditions. *Methods.* **59**, 301–315
- 28. Robinson, S. P., and Giersch, C. (1987) Inorganic Phosphate Concentration in the Stroma of Isolated Chloroplasts and Its Influence on Photosynthesis. *Funct. Plant Biol.* **14**, 451–462
- 29. Robinson, S. P., and Downton, W. J. S. (1984) Potassium, sodium, and chloride content of isolated intact chloroplasts in relation to ionic compartmentation in leaves. *Arch. Biochem. Biophys.* **228**, 197–206
- 30. Zhao, D., Oosterhuis, D. M., and Bednarz, C. W. (2001) Influence of Potassium Deficiency on Photosynthesis, Chlorophyll Content, and Chloroplast Ultrastructure of Cotton Plants. *Photosynthetica*. **39**, 103–109

- 31. Mizuguchi, M., Kroon, G. J., Wright, P. E., and Dyson], H. [Jane (2003) Folding of a β-sheet Protein Monitored by Real-time NMR Spectroscopy. *J. Mol. Biol.* **328**, 1161–1171
- 32. Zeeb, M., Rosner, H., Zeslawski, W., Canet, D., Holak, T. A., and Balbach, J. (2002) Protein folding and stability of human CDK inhibitor p19(INK4d). *J Mol Biol.* **315**, 447–457
- 33. Sakurai, K., and Goto, Y. (2007) Principal component analysis of the pH-dependent conformational transitions of bovine beta-lactoglobulin monitored by heteronuclear NMR. *Proc Natl Acad Sci U S A.* **104.** 15346–15351
- 34. Xu, J., and Van Doren, S. R. (2017) Tracking Equilibrium and Nonequilibrium Shifts in Data with TREND. *Biophys. J.* **112**, 224–233
- 35. Xu, J., and Van Doren, S. R. (2018) Affinities and Comparisons of Enzyme States by Principal Component Analysis of NMR Spectra, Automated Using TREND Software. in *Methods in Enzymology*, pp. 217–240, Academic Press, **607**, 217–240
- 36. Xu, J., and Van Doren, S. R. (2016) Binding Isotherms and Time Courses Readily from Magnetic Resonance. *Anal. Chem.* **88**, 8172–8178
- 37. Xu, J., Sarma, A. V. S., Wei, Y., Beamer, L. J., and Van Doren, S. R. (2017) Multiple Ligand-Bound States of a Phosphohexomutase Revealed by Principal Component Analysis of NMR Peak Shifts. *Sci. Rep.* **7**, 5343
- 38. Zhang, Y., Mun, S. R., Linares, J. F., Ahn, J., Towers, C. G., Ji, C. H., Fitzwalter, B. E., Holden, M. R., Mi, W., Shi, X., Moscat, J., Thorburn, A., Diaz-Meco, M. T., Kwon, Y. T., and Kutateladze, T. G. (2018) ZZ-dependent regulation of p62/SQSTM1 in autophagy. *Nat. Commun.* **9**, 4373
- 39. Namanja, A. T., Xu, J., Wu, H., Sun, Q., Upadhyay, A. K., Sun, C., Van Doren, S. R., and Petros, A. M. (2019) NMR-based fragment screening and lead discovery accelerated by principal component analysis. *J. Biomol. NMR*. **73**, 675–685
- 40. Karki, N., and Bates, P. D. (2018) The effect of light conditions on interpreting oil composition engineering in Arabidopsis seeds. *Plant Direct.* **2**, e00067
- 41. Armbruster, U., Correa Galvis, V., Kunz, H.-H., and Strand, D. D. (2017) The regulation of the chloroplast proton motive force plays a key role for photosynthesis in fluctuating light. *Curr. Opin. Plant Biol.* **37**, 56–62
- 42. Hashida, S., and Kawai-Yamada, M. (2019) Inter-Organelle NAD Metabolism Underpinning Light Responsive NADP Dynamics in Plants. *Front. Plant Sci.* **10**, 960
- 43. Portis, A. R., and Heldt, H. W. (1976) Light-dependent changes of the Mg2+ concentration in the stroma in relation to the Mg2+ dependency of CO2 fixation in intact chloroplasts. *Biochim. Biophys. Acta Bioenerg.* **449**, 434–446
- 44. Fall, R. R. (1976) Stabilization of an acetyl-coenzyme a carboxylase complex from Pseudomonas citronellolis. *Biochim. Biophys. Acta Lipids Lipid Metab.* **450**, 475–480
- 45. Choi-Rhee, E., and Cronan, J. E. (2003) The Biotin Carboxylase-Biotin Carboxyl Carrier Protein Complex of Escherichia coli Acetyl-CoA Carboxylase. *J. Biol. Chem.* . **278**, 30806–30812
- 46. Wright, P. E., and Dyson, H. J. (2015) Intrinsically disordered proteins in cellular signalling and regulation. *Nat. Rev. Mol. Cell Biol.* **16**, 18–29
- 47. BURGEN, A. S. V., ROBERTS, G. C. K., and FEENEY, J. (1975) Binding of flexible ligands

- to macromolecules. Nature. 253. 753-755
- 48. Williamson, M. P. (2012) *How Proteins Work*, Garland Science, Taylor & Francis Group, LLC, New York
- 49. Shoemaker, B. A., Portman, J. J., and Wolynes, P. G. (2000) Speeding molecular recognition by using the folding funnel: The fly-casting mechanism. *Proc. Natl. Acad. Sci.* **97**, 8868–8873
- 50. Sugase, K., Dyson, H. J., and Wright, P. E. (2007) Mechanism of coupled folding and binding of an intrinsically disordered protein. *Nature*. **447**, 1021
- 51. Dosztanyi, Z., Meszaros, B., and Simon, I. (2009) ANCHOR: web server for predicting protein binding regions in disordered proteins. *Bioinformatics*. **25**, 2745–2746
- 52. Mészáros, B., Simon, I., and Dosztányi, Z. (2009) Prediction of Protein Binding Regions in Disordered Proteins. *PLoS Comput. Biol.* **5**, e1000376
- 53. Uversky, V. N. (2009) Intrinsically Disordered Proteins and Their Environment: Effects of Strong Denaturants, Temperature, pH, Counter Ions, Membranes, Binding Partners, Osmolytes, and Macromolecular Crowding. *Protein J.* **28**, 305–325
- 54. Liu, J., Faeder, J. R., and Camacho, C. J. (2009) Toward a quantitative theory of intrinsically disordered proteins and their function. *Proc. Natl. Acad. Sci. U. S. A.* **106**, 19819–19823
- 55. Sievers, F., Wilm, A., Dineen, D., Gibson, T. J., Karplus, K., Li, W., Lopez, R., McWilliam, H., Remmert, M., Söding, J., Thompson, J. D., and Higgins, D. G. (2011) Fast, scalable generation of high-quality protein multiple sequence alignments using Clustal Omega. *Mol. Syst. Biol.* **7**, 539
- 56. Schwede, T., Kopp, J., Guex, N., and Peitsch, M. C. (2003) SWISS-MODEL: An automated protein homology-modeling server. *Nucleic Acids Res.* **31**, 3381–3385
- 57. Waterhouse, A., Bertoni, M., Bienert, S., Studer, G., Tauriello, G., Gumienny, R., Heer, F. T., de Beer, T. A. P., Rempfer, C., Bordoli, L., Lepore, R., and Schwede, T. (2018) SWISS-MODEL: homology modelling of protein structures and complexes. *Nucleic Acids Res.* **46**, W296–W303
- 58. DeLano, W. L. (2002) The PyMOL Molecular Graphics System
- 59. Robert, X., and Gouet, P. (2014) Deciphering key features in protein structures with the new ENDscript server. *Nucleic Acids Res.* **42**, W320–W324
- 60. Gasteiger, E., Hoogland, C., Gattiker, A., Duvaud, S., Wilkins, M. R., Appel, R. D., and Bairoch, A. (2005) No Title. in *The Proteomics Protocols Handbook*, pp. 571–607
- 61. Emanuelsson, O., Nielsen, H., and Heijne, G. Von (1999) ChloroP, a neural network-based method for predicting chloroplast transit peptides and their cleavage sites. *Protein Sci.* **8**, 978–984
- 62. van Holde, K. E., Johnson, C. W. J., and Ho, P. S. (1998) *Principles of Physical Biochemistry*, 1st Ed., Prentice Hall, Upper Saddle River, NJ, 0
- 63. Yabuta, Y., Tamoi, M., Yamamoto, K., Tomizawa, K., Yokota, A., and Shigeoka, S. (2008) Molecular Design of Photosynthesis-Elevated Chloroplasts for Mass Accumulation of a Foreign Protein. *Plant Cell Physiol.* **49**, 375–385
- 64. Studier, F. W. (2005) Protein production by auto-induction in high-density shaking cultures.

- Protein Expr. Purif. **41**, 207–234
- 65. Farjon, J., Boisbouvier, J., Schanda, P., Pardi, A., Simorre, J. P., and Brutscher, B. (2009) Longitudinal-relaxation-enhanced NMR experiments for the study of nucleic acids in solution. *J Am Chem Soc.* **131**, 8571–8577
- 66. Tanford, C. (1970) Protein Denaturation: Part C.\*\*Parts A and B were published in Volume 23 of Advances in Protein Chemistry (1968), starting on p. 121 Theoretical Models for The Mechanism of Denaturation (Anfinsen, C. B., Edsall, J. T., and Richards, F. M. eds), pp. 1–95, Advances in Protein Chemistry, Academic Press, **24**, 1–95
- 67. Taulier, N., and Chalikian, T. V (2001) Characterization of pH-induced transitions of β-lactoglobulin: ultrasonic, densimetric, and spectroscopic studies11Edited by C. R. Matthews. *J. Mol. Biol.* **314**, 873–889
- 68. Li, Y., Beisson, F., Pollard, M., and Ohlrogge, J. (2006) Oil content of Arabidopsis seeds: The influence of seed anatomy, light and plant-to-plant variation. *Phytochemistry*. **67**, 904–915
- 69. Lescop, E., Kern, T., and Brutscher, B. (2010) Guidelines for the use of band-selective radiofrequency pulses in hetero-nuclear NMR: example of longitudinal-relaxation-enhanced BEST-type 1H-15N correlation experiments. *J Magn Reson.* **203**, 190–198

### **FOOTNOTES**

This work was supported by NSF grant MCB 1716688.

The abbreviations used are: AQUA-MRM, absolute quantitation - multiple reaction monitoring; BADC, biotin attachment domain-containing; BC, biotin carboxylase; BCCP, biotin carboxyl carrier protein; CT, carboxyltransferase; FA, fatty acid; FAME, fatty acyl methyl ester; hetACCase, heteromeric acetyl-CoA carboxylase; IDR, intrinsically disordered region; MST, microscale thermophoresis; NMR, nuclear magnetic resonance spectroscopy; PBS, phosphate-buffered saline; PBK, phosphate buffer with KCl; TREND, software for tracking equilibrium and non-equilibrium shifts in data; TROSY, transverse relaxation optimized spectroscopy

Table 1. Apparent affinities for the BC subunit measured in selected solution conditions by microscale thermophoresis <sup>A</sup>.

	HEPES, pH 7,	HEPES, pH 8,	PBS, pH 7	PBS, pH 8	PBK, pH 8
	KCI	KCI			
BCCP1 K <sub>D</sub> , M	4.4 ± 0.9E-8	4.6 ± 0.5E-8	3.6 ± 0.6E-7	1.9 ± 0.3E-6	6.9 ± 0.6E-7
ΔG, kcal/mol	-10.0 ± 0.1	-10.0 ± 0.1	-8.8 ± 0.1	-7.8 ± 0.1	-8.4 ± 0.1
BCCP2 K <sub>D</sub> , M	1.5 ± 0.4E-7	2.6 ± 0.8E-7	4.6 ± 0.5E-7	3.3 ± 0.2E-6	4.7 ± 0.9E-7
ΔG, kcal/mol	-9.3 ± 0.1	-9.0 ± 0.1	-8.6 ± 0.1	-7.5 ± 0.1	-8.6 ± 0.1
BADC1 K <sub>D</sub> , M	5.8 ± 2.3E-7	4.7 ± 0.6E-6	$5.4 \pm 1.7E-8^{B}$	1.9 ± 0.5E-6	8.8 ± 2.2E-6
ΔG, kcal/mol	-8.5 ± 0.2	-7.3 ± 0.1	$-9.9 \pm 0.1^{B}$	-7.8 ± 0.1	-6.9 ± 0.1
BADC2 K <sub>D</sub> , M	1.85 ± 0.2E-7	5.1 ± 2.3E-7	1.5 ± 0.3E-7	5.8 ± 1.0E-7	7.1 ±1.1E-7
ΔG, kcal/mol	-9.2 ± 0.1	-8.6 ± 0.2	-9.3 ± 0.1	-8.5 ± 0.1	-8.4 ± 0.1
BADC3 K <sub>D</sub> , M	1.7 ± 0.4E-6	2.9 ± 0.9E-6	3.6 ± 0.8E-7	1.8 ± 0.2E-6	5.0 ± 1.1E-7
ΔG, kcal/mol	-7.9 ± 0.1	-7.6 ± 0.1	-8.8 ± 0.1	-7.8 ± 0.1	-8.6 ± 0.1

<sup>&</sup>lt;sup>A</sup> Uncertainties in the curve fits are listed. The titrations were performed in triplicate.

<sup>&</sup>lt;sup>B</sup> Required a second, lower affinity association (not listed) for an acceptable fit; see Fig. 2.

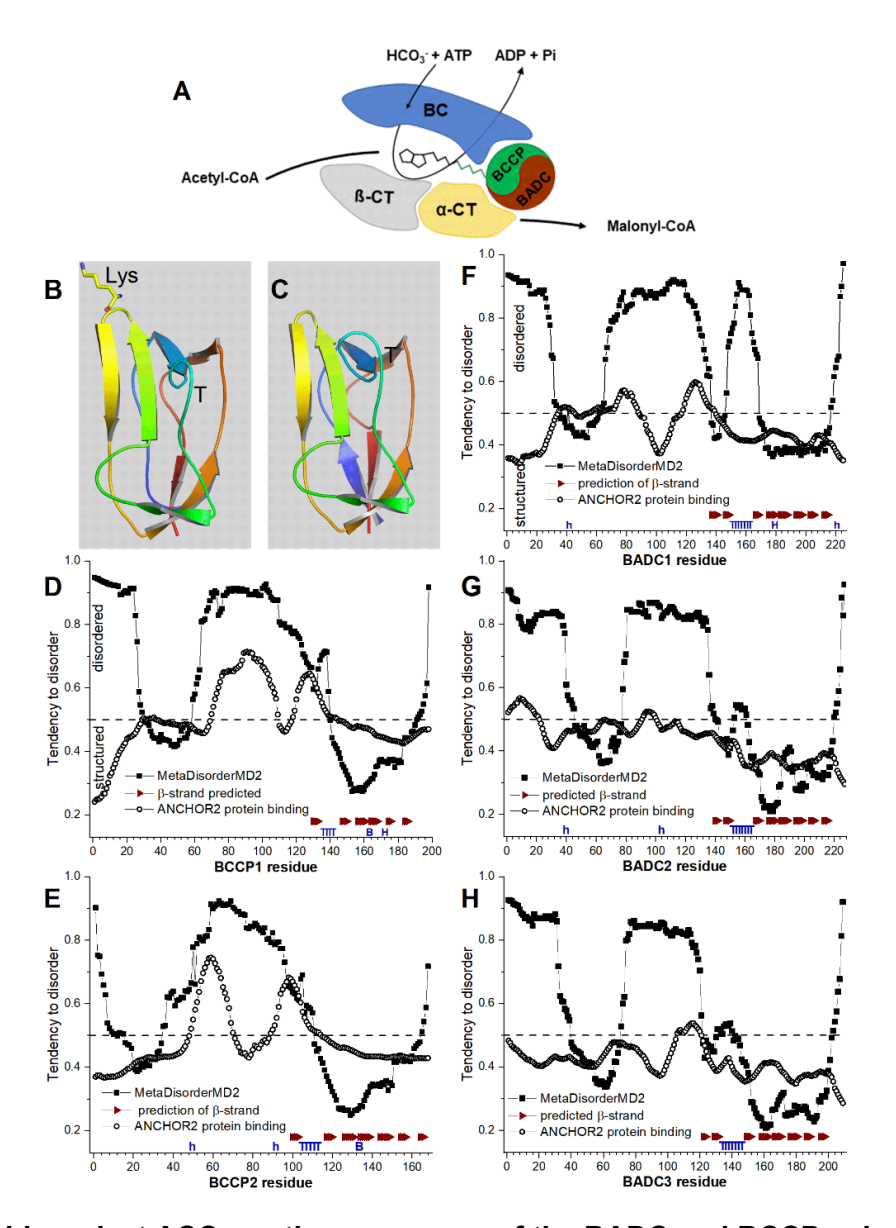


Figure 1. In chloroplast ACCase, the sequences of the BADC and BCCP subunits suggest both folded and disordered regions. (A) The cartoon of hetero ACCase indicates the types of subunits in the biotin carboxylase and carboxyltransferase subcomplexes, as well as the overall reaction. *Panels B and C* plot homology models of the folded domains of BCCP2 (B) and BADC1 (C) from *A. thaliana*. The ribbon is colored the spectrum from purple at the N-terminal end to red at the C-terminus. *Panels D to H* plot order predictions by MetaDisorderMD2 (using multiple algorithms at the GeneSilico server) with black squares vs. sequence numbering of the mature forms of the BCCP1 (D), BCCP2 (E), BADC1 (F), BADC2 (G), and BADC3 (H) subunits. Values > 0.5 are considered disordered. ANCHOR2 (open circles) predicts potential regions of protein binding where the values exceed 0.5. The location of β-strands predicted by homology modeling using the EXPASY server are marked with arrowheads. "T" marks residues predicted to be part of the loop called the thumb. "B" represents the lysine that becomes biotinylated. A histidine is marked "H" in the folded region or "h" in an unfolded region.

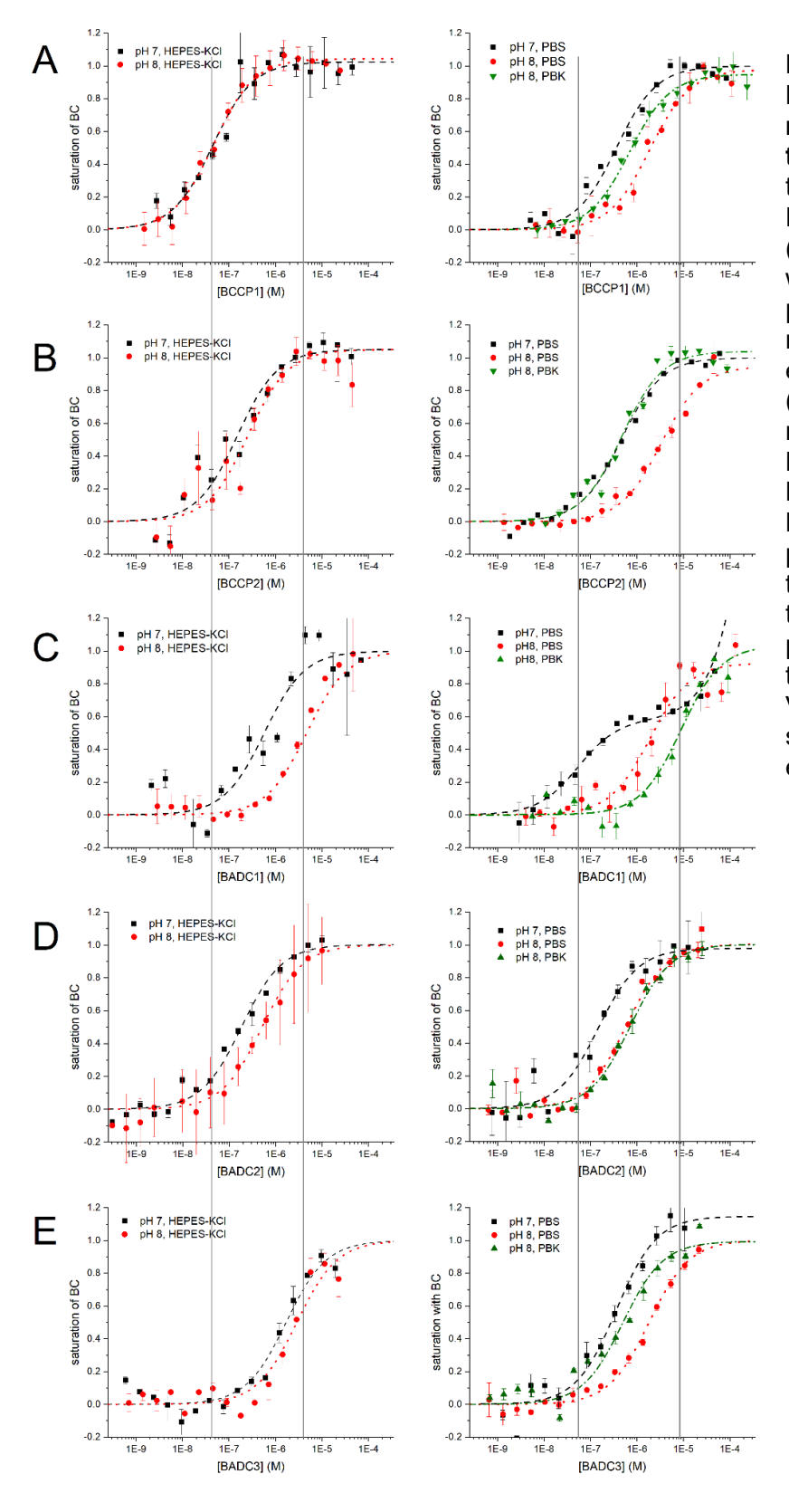


Figure 2. Affinities for BC of **BADC** and **BCCP** subunits measured by microscale thermophoresis (MST). The titrations were measured in HEPES buffer with 140 mM KCl (left panels) or phosphate buffer with 140 mM NaCl or KCl (right panels), with n = 3 technical replicates providing the S.D. of each point. Recombinant BC (19.5 nM) was titrated by recombinant BCCP1 (A), BCCP2 BADC1 (B), (C), BADC2 (D), or BADC3 (E). Black squares mark titrations at pH 7.0. Red circles mark titrations at pH 8.0. Green triangles mark titrations in phosphate buffer named PBK that replaces NaCl with KCl. Vertical gray lines mark the strongest and weakest  $K_D$  in each column of panels.

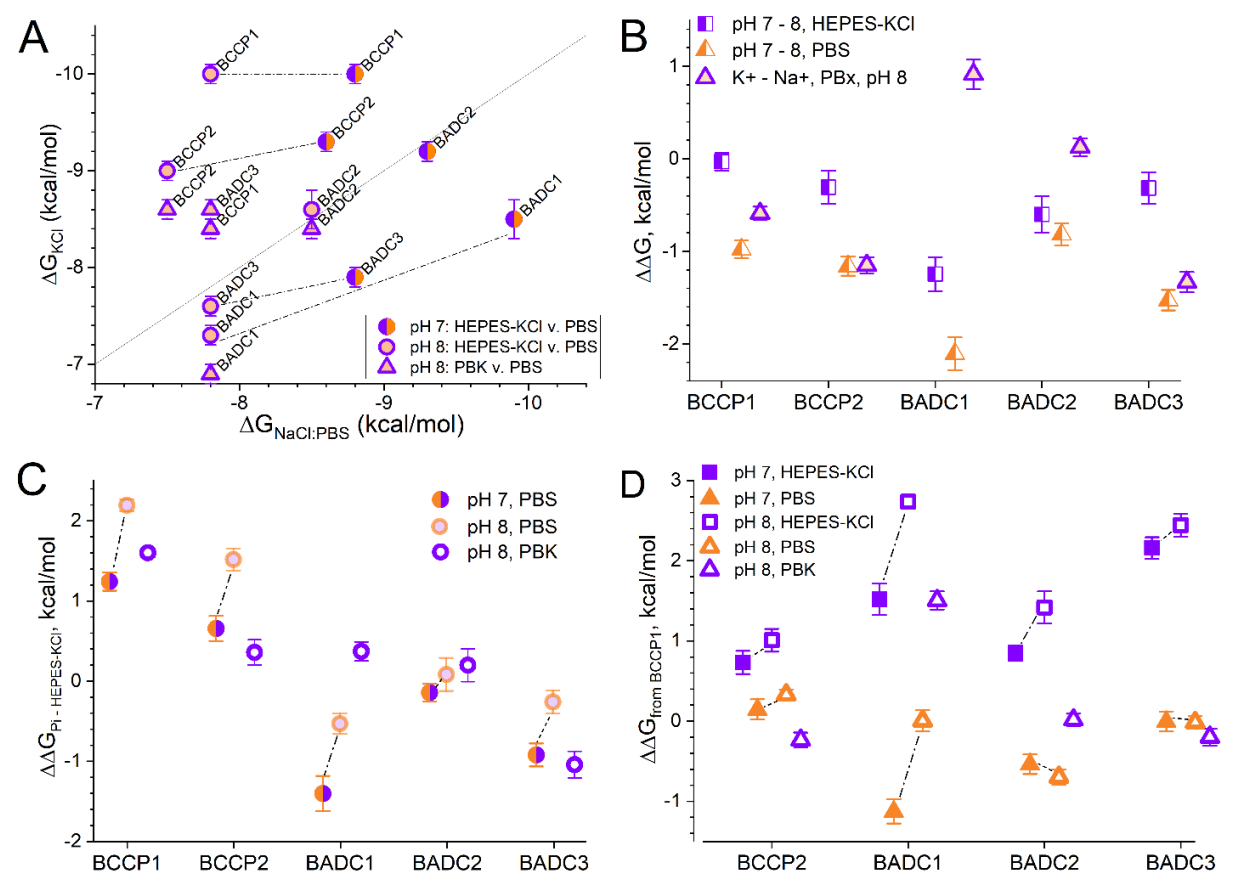


Figure 3. Dependence of affinities for BC on pH, buffer, cation, and partner subunit. Gibbs free energies of the associations between the BC subunit and each of the BCCP or BADC subunits are from the  $K_D$  values fitted to the titrations plotted in Fig. 2 and listed in Table 1. The buffer ion is symbolized by shape of the symbol with a square representing HEPES, a triangle for phosphate buffer, and a circle comparing phosphate with HEPES. Open symbols represent pH 8, filled symbols pH 7. Orange represents Na<sup>+</sup> ions present and violet for K<sup>+</sup> ions. More negative quantities denote higher affinity for BC. Dashed lines connect results at pH 7 and 8. (A) Affinities for BC are compared between KCl and NaCl solutions. Comparison of Na<sup>+</sup> and K<sup>+</sup> ions at pH 7 is colored half orange and half violet. Comparison of Na<sup>+</sup> and K<sup>+</sup> ions at pH 8 is colored on the perimeter to represent K<sup>+</sup> and in the interior to represent Na<sup>+</sup>. The diagonal line marks equivalence in affinity. (B) The effects of pH and cation are compared again as differences ( $\Delta\Delta G$ ) from titrations in buffer at pH 8. Half-filled, half-open symbols compare pH 7 with pH 8 as reference. A negative value means the titration displayed greater affinity than that of the titration at pH 8. The titration in PBS at pH 8 is the reference for the titration in PBK at pH 8. (C) The difference in binding free energy between that in the phosphate buffer and that in HEPES buffer at the same pH is plotted for each of the titrations of BC with a small subunit. The two-color code is that of panel A. (D) The difference in the binding free energy is plotted, relative to BCCP1 titrations, for each of the five buffer compositions used in the titrations. A negative  $\Delta\Delta G$  specifies higher affinity than in the BC titration with BCCP1. The error bars reflect uncertainties in curve fitting and propagation of the errors through differences between titrations.

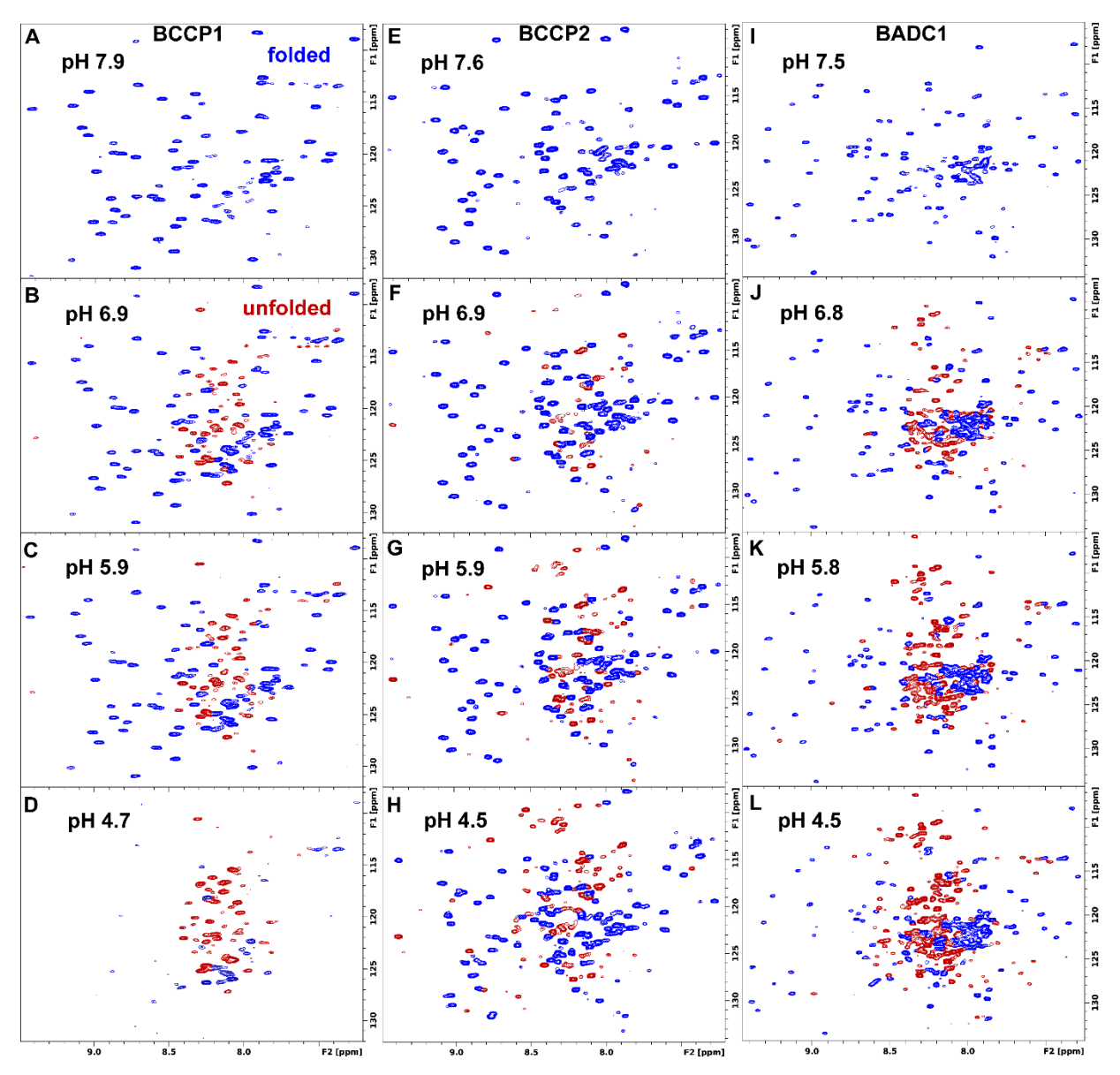
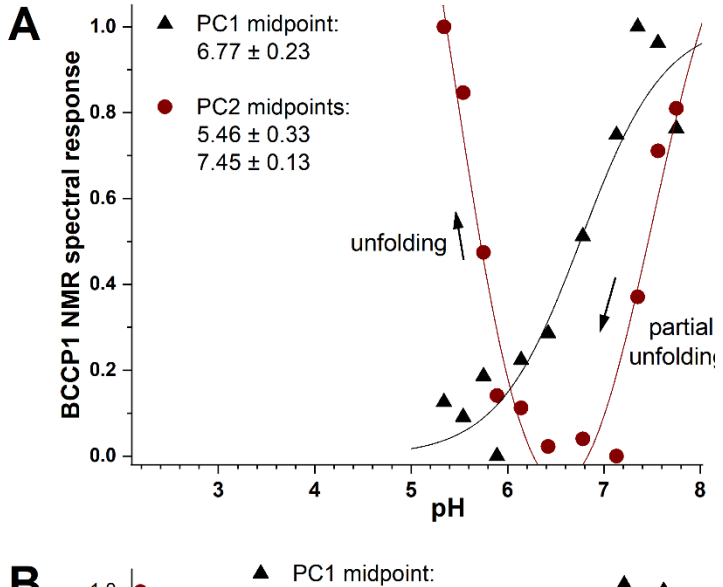
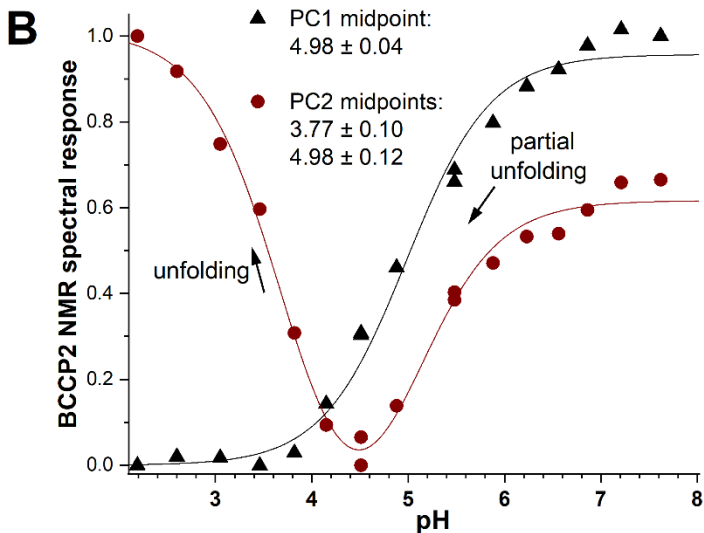


Figure 4. Amide NMR spectra observe partial unfolding at the near-neutral end of the physiological pH range. Amide NMR spectra from pH titrations of (A-D) BCCP1, (E-H) BCCP2, and (I-L) BADC1 were collected on  $^{15}\text{N}$ -labeled samples of 150 to 180  $\mu\text{M}$  in PBS buffer at 800 MHz using the BEST-TROSY pulse sequence of ref (69). The peaks with the blue contours represent the folded domain that predominates in the spectra under weakly basic conditions. The peaks with red contours appear under neutral to acidic conditions and are attributable to partial unfolding. Complete unfolding of BCCP1 is observed at pH 4.7 in panel D.





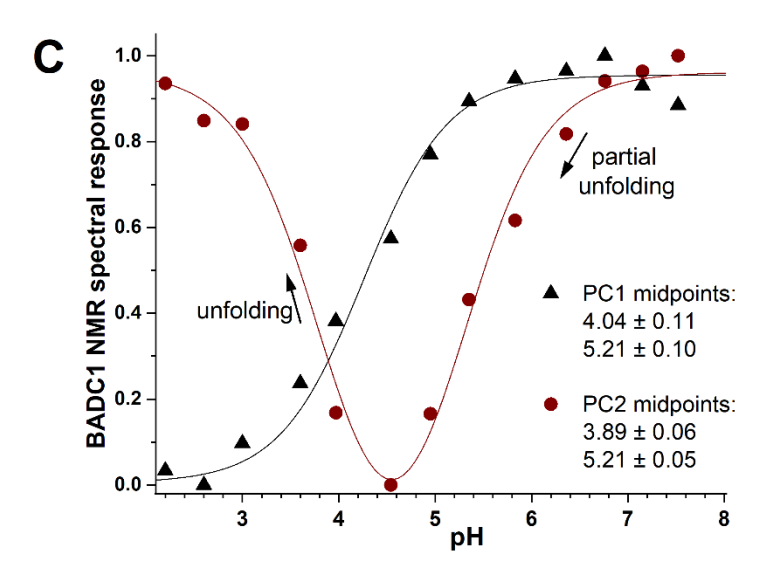
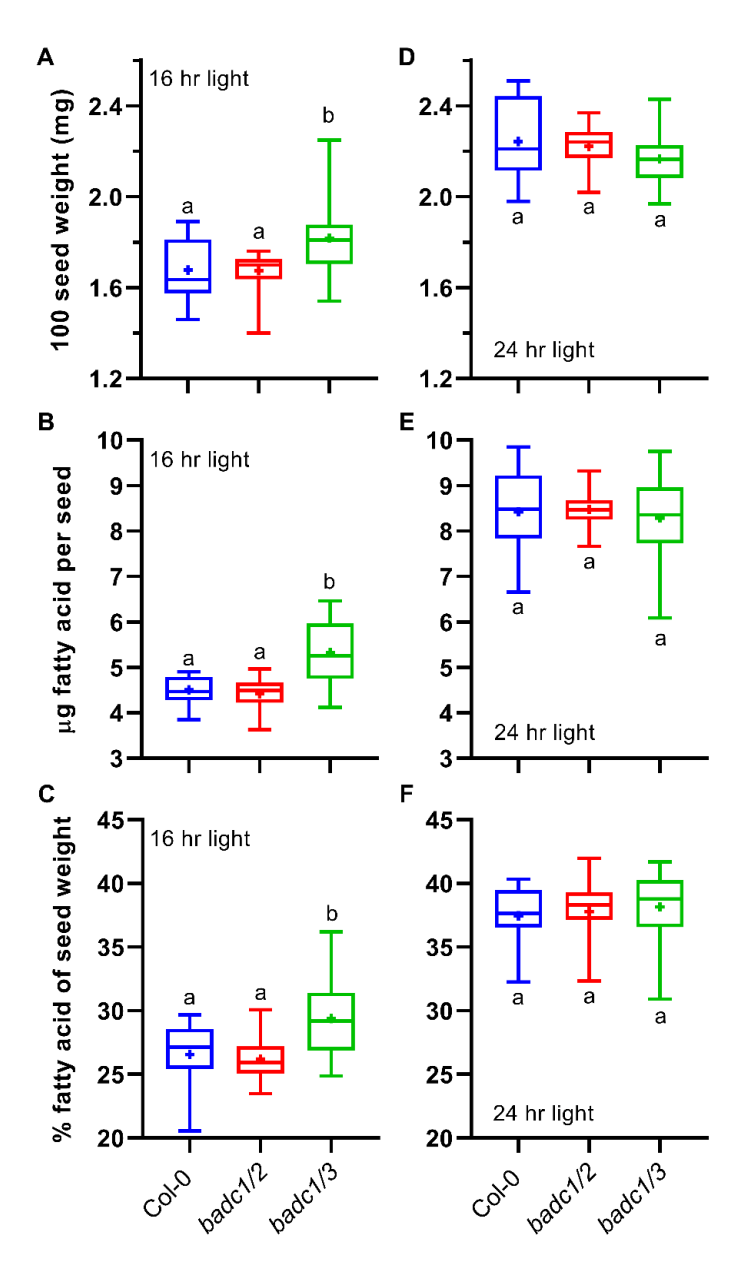


Figure 5. The pH dependence of NMR spectra finds BCCP1 more sensitive to unfolding by mild acidification than BCCP2 or BADC1. The largest trends of pH-dependent change of (A) BCCP1, (B) BCCP2, and (C) BADC1 were derived as principal components (PCs) directly from the <sup>15</sup>N BEST-TROSY spectra (34, 36). PC1 is marked with black triangles and PC2 with red circles. PC1 was fitted to eq. 4 and PC2 fitted to eq. 5 using TREND NMR software (35). The midpoints of the fitted pH-dependent changes are listed with the uncertainties in the fits. The curves fit the data points with R<sup>2</sup> of 0.93, 0.99, and 0.98 for BCCP1, BCCP2, and BADC1, respectively. The changes in the appearance of the NMR spectra are attributable to partial unfolding, or complete unfolding of the structured domain at lower pH.



**Figure 6.** Increase in seed oil content of the Arabidopsis *badc1 badc3* mutant depends on light conditions during growth. Wild-type (Col-0, blue) and the double mutants *badc1 badc2* (*badc1/2*, red) and *badc1 badc3* (*badc1/3*, green) were grown together in a 16/8 hr light/dark cycle (A-C), or under 24 hr constant light (D-F). Harvested seeds were analyzed for seed weight (A, D), fatty acid content per seed (B, E), and fatty acid content as a percentage of seed weight (C, F). Each measurement utilized 100 seeds from a single plant, and 15-18 separate individual plant replicates. Box-and-whisker plot: box, 25<sup>th</sup> to 75<sup>th</sup> percentile; line, median; +, mean; whiskers, the range minimum to maximum. Significant differences between lines (one-way ANOVA, p-value < 0.05) are indicated by differing letters.

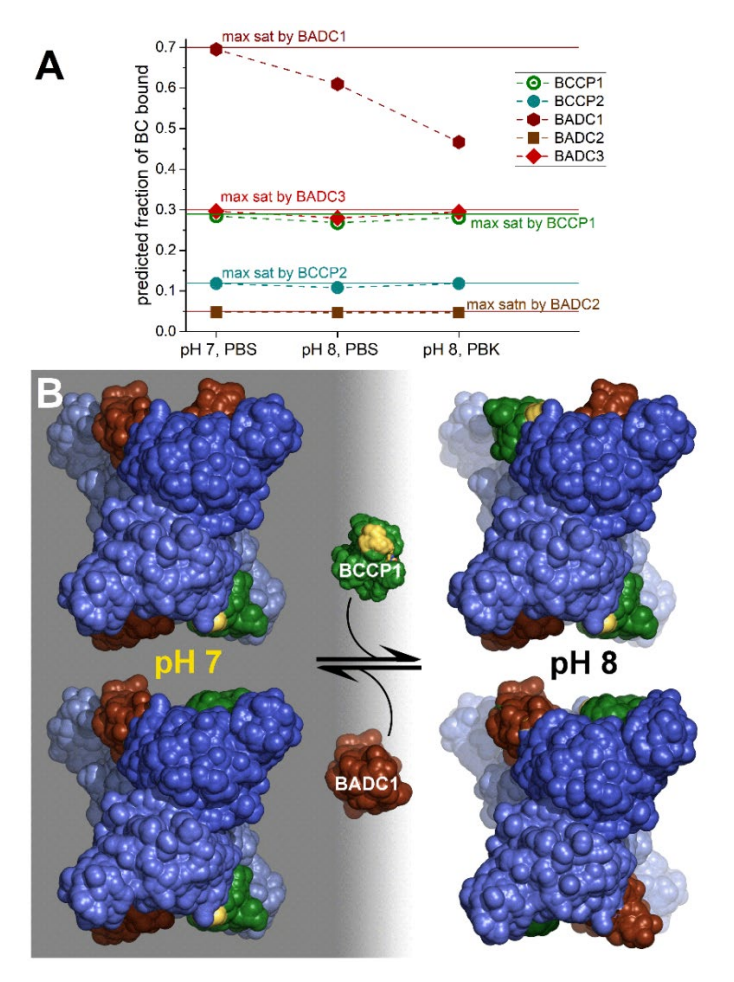


Figure 7. Predicted shifts in occupation of BC by BADC1 and BCCP1 between dark conditions of pH 7 and daylight conditions of pH 8. This prediction is based on the BC affinities for BCCP and BADC subunits, protein levels of these subunits during development of seeds in Arabidopsis siliques (19), and the simplifying assumption that the small subunit binds independently to BC. (A) The saturation of BC by each subunit is calculated using eq. 3,  $K_D$ measured in phosphate solution (Table 1), and the subunit concentrations in siliques given in Table S1, scaled up by the 400 mg/ml of protein present in plastids (63). The horizontal lines indicate the maximum possible levels of saturation of BC by that subunit based on the concentrations in Table S1. (B) The anticipated pH-dependent shift in the equilibrium binding of BC by the BADC1 and BCCP1 subunits that are abundant in plastids is depicted The crystallographic coordinates (PDB: 4HR7) of the BC subcomplex from E. coli (16) shows a tetramer of BC subunits in shades of blue and the folded domain of the BCCP subunits in green with the conserved site of biotinylation (sequence of MKM) colored yellow. The homology model of the folded domain of BADC1 (brown) from Arabidopsis is superimposed on selected BCCP chains bound to a BC subunit in the crystal structure. Arabidopsis BCCP1 chains are represented by the E. coli BCCP chains (green) in the crystal structure. This overly simplified representation of the BC subcomplex in Arabidopsis plastids does not portray the range of oligomerization states. associations with other BADC and BCCP subunits, their intrinsic disorder, and the anticipated complexity of the mixtures of structural ensembles.